

# Recovery of the Shape of the Mass Power Spectrum from the Lyman-alpha Forest

Lam Hui<sup>1</sup>

NASA/Fermilab Astrophysics Center  
Fermi National Accelerator Laboratory, Batavia, IL 60510

## ABSTRACT

We propose a method for recovering the shape of the mass power spectrum on large scales from the transmission fluctuations of the Lyman-alpha forest, which takes into account directly redshift-space distortions. The procedure, in discretized form, involves the inversion of a triangular matrix which projects the mass power spectrum in 3-D real-space to the transmission power spectrum in 1-D redshift-space. We illustrate the method by performing a linear calculation relating the two. A method that does not take into account redshift-space anisotropy tends to underestimate the steepness of the mass power spectrum, in the case of linear distortions. The issue of the effective bias-factor for the linear distortion kernel is discussed.

*Subject headings:* cosmology: theory — intergalactic medium — quasars: absorption lines — large-scale structure of universe

## 1. Introduction

In an elegant paper, Croft et al. (1998) introduced a method for recovering the shape of the three-dimensional primordial mass power spectrum on large scales from the one-dimensional transmission power spectrum of the Lyman-alpha forest. They observed that the two are related by an integral of the form:

$$P(k_{\parallel}) \propto \int_{k_{\parallel}}^{\infty} \tilde{P} \frac{k dk}{2\pi} \quad (1)$$

where  $k_{\parallel}$  is the wave-vector along the line of sight,  $k$  is the magnitude of the three-dimensional wave-vector, and  $P$  and  $\tilde{P}$  are the one-dimensional redshift-space transmission power spectrum and the three-dimensional redshift-space mass power spectrum respectively. It was

---

<sup>1</sup>e-mail: [lhui@fnal.gov](mailto:lhui@fnal.gov)

suggested that redshift distortions merely change the normalization of  $\tilde{P}$  from its real-space counterpart, and so a simple differentiation of  $P$  would suffice in recovering the shape of the three-dimensional real-space mass power spectrum.<sup>2</sup>

Redshift distortions (see Hamilton 1997 and references therein), however, imply that  $\tilde{P}$  is in general a function of  $k_{\parallel}$  as well as  $k$ , in which case differentiation of  $P$  alone would not recover the true shape of the three-dimensional real-space mass power spectrum.

We show in §3 how to perform the inversion from the one-dimensional redshift-space transmission power spectrum to the three-dimensional real-space mass power spectrum correctly, for general, not necessarily linear, redshift distortions. It involves the inversion of a triangular matrix, which acts as a distortion kernel. We illustrate the method in §4 with a perturbative example (i.e linear distortions), and demonstrate that the method of simple differentiation generally outputs a real-space mass power spectrum which is flatter than the true one. We end with some concluding remarks in §5.

Before we proceed, however, let us clarify our notation on the various power spectra treated in this paper.

## 2. A Note on Notation

To avoid a proliferation of superscripts and subscripts, we adopt the following convention for the various power spectra,  $P$ , discussed in this paper. We use  $\tilde{\phantom{P}}$  to distinguish between one-dimensional and three-dimensional power spectra:  $P$  is 1-D and  $\tilde{P}$  is 3-D (i.e.  $P$  has a dimension which is the cube-root of that of  $\tilde{P}$ ). To distinguish between the three-dimensional redshift-space (anisotropic) versus the three-dimensional real-space (isotropic) power spectra, we rely on either the context or explicit arguments of the power spectra: the former is denoted by  $\tilde{P}(k_{\parallel}, k)$  while the latter, being isotropic, is denoted simply by  $\tilde{P}(k)$ . In this paper, all one-dimensional power spectra, on the other hand, are implicitly in redshift-space. Finally, to tell apart the power spectrum of density from that of transmission/flux, we use superscripts:  $P^{\rho}$  versus  $P^f$ , where  $\rho$  denotes the density and  $f$  the transmission.

---

<sup>2</sup>Croft et al. (1998) in fact differentiated the Gaussianized transmission power spectrum rather than the transmission power spectrum itself. Their investigation seems to indicate that the two give very similar results, except that the former yields smaller error-bars. We will consider the non-Gaussianized version of their method in this paper for simplicity.

### 3. General Non-perturbative Formula

The three-dimensional, generally anisotropic, power spectrum of some random field is related to its one-dimensional projection through the following integral (Kaiser & Peacock 1991)

$$P(k_{\parallel}) = \int_{k_{\parallel}}^{\infty} \tilde{P}(k_{\parallel}, k) \frac{k dk}{2\pi} \quad (2)$$

where  $k_{\parallel}$  is the wave-vector along the line of sight, and  $k$  is the magnitude of the three-dimensional wave-vector i.e.  $k^2 = k_{\parallel}^2 + k_{\perp}^2$  where  $k_{\perp}$  is the magnitude of the wave-vector perpendicular to the line of sight. We assume that  $\tilde{P}$  is independent of the direction of  $\mathbf{k}_{\perp}$ , by azimuthal symmetry, as is in the case of redshift distortions. Note that we have used  $\tilde{P}$  for the three-dimensional power spectrum, to distinguish it from  $P$ , its one-dimensional counterpart.

The power spectra are related to the three-dimensional, generally anisotropic, two-point correlation function  $\xi$  by the following:

$$\begin{aligned} P(k_{\parallel}) &= 2 \int_0^{\infty} \xi(u_{\parallel}, 0) \cos(k_{\parallel} u_{\parallel}) du_{\parallel} \\ \tilde{P}(k_{\parallel}, k) &= 4\pi \int_0^{\infty} \int_0^{\infty} \xi(u_{\parallel}, u_{\perp}) \cos(k_{\parallel} u_{\parallel}) J_0(k_{\perp} u_{\perp}) u_{\perp} du_{\perp} du_{\parallel} \end{aligned} \quad (3)$$

where  $J_0(r)$  is the zeroth order Bessel function. The two-point correlation  $\xi$  depends on the magnitude of  $\mathbf{u}_{\perp}$  but not its direction, again by azimuthal symmetry.

The  $u_{\parallel}$  coordinate above stands for the velocity along the line of sight (in  $\text{km s}^{-1}$ ) i.e.  $u_{\parallel} \equiv c(\lambda - \bar{\lambda})/\bar{\lambda}$  where  $\lambda$  is the observed wavelength,  $\bar{\lambda}$  is the mean wavelength of interest, and  $c$  is the speed of light.

The  $u_{\perp}$  coordinate stands for the transverse distance in velocity units i.e.  $u_{\perp} \equiv \bar{H} x_{\perp}/(1 + \bar{z})$ , where  $x_{\perp}$  is the actual comoving transverse distance,  $\bar{z}$  is the mean redshift of interest and  $\bar{H}$  is the Hubble parameter at that redshift. The mean redshift and the mean wavelength are related by  $\bar{\lambda} = \lambda_{\alpha}(1 + \bar{z})$ ,  $\lambda_{\alpha} = 1216 \text{ \AA}$ .

The Fourier counterparts of  $u_{\parallel}$  and  $u_{\perp}$  are  $k_{\parallel}$  and  $k_{\perp}$ . Occasionally, we will abuse the notation by using the  $(u_{\parallel}, k_{\parallel})$  pair to denote the coordinates in wavelength units i.e.  $(\lambda - \bar{\lambda})$  and its Fourier transform.

The effect of redshift-space distortions on the power spectrum, at both small and large scales, can be described by:

$$\tilde{P}(k_{\parallel}, k) = W(k_{\parallel}/k, k) \tilde{P}(k) \quad (4)$$

where  $\tilde{P}(k)$  is the isotropic power spectrum in the absence of peculiar motion, and  $W$  is a suitable distortion kernel. Note that we rely on explicitly displaying the arguments to distinguish between the isotropic and the anisotropic power spectra.

Finally, putting eq. (4) into eq. (2), it can be seen that the one-dimensional redshift-space power spectrum is related to the isotropic three-dimensional real-space power spectrum by a linear integral equation:

$$P(k_{\parallel}) = \int_{k_{\parallel}}^{\infty} W(k_{\parallel}/k, k) \tilde{P}(k) \frac{kdk}{2\pi} \quad (5)$$

Thus far, we have not specified the actual random field whose power spectrum we are interested in. The random field could be the mass overdensity  $\delta = \delta\rho/\bar{\rho}$  or the transmission/flux overdensity  $\delta_f = \delta f/\bar{f}$ , where  $f = e^{-\tau}$ ,  $\bar{f} = \langle f \rangle$ ,  $\delta f = f - \bar{f}$ , and  $\tau$  is the optical depth. We will use  $P^{\rho}$  or  $\tilde{P}^{\rho}$  to denote the mass power spectrum and  $P^f$  or  $\tilde{P}^f$  to denote the transmission power spectrum.

The one-dimensional redshift-space transmission power spectrum can also be related to the three-dimensional real-space mass power spectrum by an effective kernel, which we will call  $W^{f\rho}$ :

$$P^f(k_{\parallel}) = \int_{k_{\parallel}}^{\infty} W^{f\rho}(k_{\parallel}/k, k) \tilde{P}^{\rho}(k) \frac{kdk}{2\pi} \quad (6)$$

In discretized form, this is equivalent to:

$$\mathbf{P}^f = \mathbf{A} \cdot \tilde{\mathbf{P}}^{\rho} \quad (7)$$

where the power spectra are represented as vectors and  $\mathbf{A}$  is an upper (or lower) triangular matrix, which is invertible if none of the diagonal entries of  $\mathbf{A}$  vanishes. The special case considered by Croft et al. (1998) corresponds to  $W^{f\rho} = \text{const.}$ , where inverting the above matrix equation is equivalent to the differentiation of  $P^f(k_{\parallel})$ .

The problem of eq. (7) is of course that  $P^f(k_{\parallel})$ , for any given  $k_{\parallel}$ , depends on an infinite vector:  $\tilde{P}^{\rho}(k)$  for all  $k$ 's, from  $k_{\parallel}$  to, in principle,  $\infty$ . To make it useful for computation, we have to truncate the infinite vectors somehow. Suppose one is given a finite vector of  $P^f(k_{\parallel})$ , for  $k_{\parallel}^A \leq k_{\parallel} \leq k_{\parallel}^B$  say. Eq. (7), in component form, can be rewritten as:

$$P^f(k_{\parallel}) - \Delta = \sum_{k=k_{\parallel}}^{k_{\parallel}^B} A(k_{\parallel}, k) \tilde{P}^{\rho}(k) \quad (8)$$

where  $\Delta = \int_{k_{\parallel}^B}^{\infty} W^{f\rho}(k_{\parallel}/k, k) \tilde{P}^{\rho}(k) kdk/2\pi$ , and  $A(k_{\parallel}, k) = W^{f\rho}(k_{\parallel}/k, k) kdk/2\pi$ .  $A(k_{\parallel}, k)$  can be regarded as a triangular matrix in the sense that  $A(k_{\parallel}, k)$  can be set to zero for  $k < k_{\parallel}$  by the virtue of the lower limit of summation in eq. (8).

By inverting eq. (8), we can in principle determine  $\tilde{P}^\rho(k)$ , with  $\Delta$  left as a free parameter. We can do better, however, by the following observation: since  $\tilde{P}^\rho(k)$  is generally a rapidly decreasing function of  $k$  for sufficiently high  $k$ 's ( $\sim k^{-3}$ , or faster if  $\rho$  is equated with the baryon density, see footnote in §4.2), assuming  $W^{f\rho}(k_\parallel/k, k)$  does not increase significantly with  $k$ , one can see that  $\Delta$  can be made small by choosing a sufficiently high truncation  $k_\parallel^B$ . Therefore, inverting eq. (8) by ignoring  $\Delta$  altogether would still give accurate estimates of  $\tilde{P}^\rho(k)$  for  $k$ 's sufficiently smaller than  $k_\parallel^B$ . We will illustrate this with an explicit example of  $\mathbf{A}$  or  $W^{f\rho}$  in the next section.

#### 4. A Perturbative Example

In this section, we will perform a linear calculation of  $P^f$ , and we will assume the actual shape of  $P^f$  on large scales, even in the presence of nonlinearities on small scales, agrees with that of the linear prediction, while its amplitude might not. This is in the spirit of Croft et al. (1998) who argued that, ignoring redshift-distortions,  $P^f$  should be proportional to the linear  $P^\rho$  on large scales, even though the mass fluctuations have gone nonlinear on small scales. The reader is referred to Scherrer & Weinberg (1997) for arguments on why that is reasonable, in the context of local-biasing (the mapping from  $\delta$  to the optical depth or transmission can be seen as some kind of local-biasing; see §5 for subtleties however).

The output of our calculation would be a distortion kernel  $W^{f\rho}$  (eq. [6]), which may or may not be the true kernel on large scales if the mass density field has already gone nonlinear on small scales. We will have some more to say about this in §5. Nonetheless, it is unlikely that the true  $W^{f\rho}$  is equal to a simple constant i.e. the general method of inverting a triangular matrix outlined in eq. (7) should be used, rather than mere differentiation. The perturbative example set forth in this section should be seen as an illustration of the method.

##### 4.1. Linear Fluctuations

To derive the linear theory limit of  $P^f$ , let us start with the following general expression for the optical depth (see e.g. Miralda-Escude & Rees 1993; Hui et al. 1997):

$$\tau(u_\parallel) = \sum \int \frac{n_{\text{HI}}}{1 + \bar{z}} \left| \frac{ds_\parallel}{dx_\parallel} \right|^{-1} \sigma_\alpha ds_\parallel, \quad \sigma_\alpha = \sigma_{\alpha 0} \frac{c}{b_T \sqrt{\pi}} \exp[-(s_\parallel - u_\parallel)^2 / b_T^2], \quad (9)$$

where  $n_{\text{HI}}$  is the proper number density of neutral hydrogen,  $\bar{z}$  is the mean redshift of interest,  $x_\parallel$  is the comoving spatial coordinate and the integration is done over the velocity  $s_\parallel$  along the line of sight. Velocity is related to distance by  $s_\parallel = x_\parallel \bar{H} / (1 + \bar{z}) + v_{\text{pec}}(x_\parallel)$  where  $v_{\text{pec}}$

is the peculiar velocity along the line of sight, and  $x_{\parallel} = 0$  is the position where the redshift due to the Hubble expansion alone coincides exactly with  $\bar{z}$ . The Jacobian  $|ds_{\parallel}/dx_{\parallel}|^{-1}$  multiplying the proper density  $n_{\text{HI}}$  gives us the neutral hydrogen density in velocity-space, and the summation is over multiple streams of  $x_{\parallel}$ 's at a given  $s_{\parallel}$ .

The thermal profile is given in the second equality, with  $\sigma_{\alpha 0}$  being the Lyman-alpha cross section constant (Rybicki & Lightman 1979). The width of the profile is  $b_T = \sqrt{2k_B T/m_p}$  where  $T$  is the temperature of the gas,  $k_B$  is the Boltzmann constant and  $m_p$  is the mass of a proton.

Three pieces of physics remain to be specified if one were to relate the optical depth and the mass distribution: 1) ionization equilibrium implies that  $n_{\text{HI}} \propto [1 + \delta_b]^2 T^{-0.7}$ , where  $\delta_b$  is the baryon overdensity; 2) the temperature-density relation  $T = T_0(1 + \delta_b)^{\gamma-1}$ , where  $T_0$  is the mean temperature at  $\delta_b = 0$  and  $\gamma$  is determined by reionization history (Hui & Gnedin 1997); 3) the baryon distribution is smoothed on small scales with respect to the mass distribution ( $\delta_b \leftrightarrow \delta$ ; see below).

Without giving further details (see Hui & Rutledge 1997), in the weak perturbation limit ( $\delta_{\tau} \ll 1$  where  $\delta_{\tau} = (\tau - \bar{\tau})/\bar{\tau}$ ), it can be shown that:

$$\begin{aligned} \delta_{\tau}(u_{\parallel}) &= \int \left[ [2 - 0.7(\gamma - 1)]\delta_b - \frac{\partial v_{\text{pec}}}{\partial s_{\parallel}} + (\gamma - 1) \frac{b_{T_0}^2}{4} \frac{\partial^2 \delta_b}{\partial s_{\parallel}^2} \right] W(s_{\parallel} - u_{\parallel}) ds_{\parallel} , \\ W(s_{\parallel} - u_{\parallel}) &\equiv \frac{1}{b_{T_0} \sqrt{\pi}} \exp[-(s_{\parallel} - u_{\parallel})^2 / b_{T_0}^2] , \end{aligned} \quad (10)$$

where  $b_{T_0} = \sqrt{2k_B T_0/m_p}$  is the thermal broadening width at temperature  $T_0$ , and  $W$  is simply a Gaussian smoothing window.

Using the fact that  $\delta_f \propto \delta_{\tau}$  to linear order ( $\delta_f = (f - \bar{f})/\bar{f}$ , with  $f = e^{-\tau}$ ), we can deduce the one-dimensional power spectrum of the transmission:

$$P^f(k_{\parallel}) = A \exp[-k_{\parallel}^2/k_{\parallel}^2] \int_{k_{\parallel}}^{\infty} \left[ [2 - 0.7(\gamma - 1)] + f_{\Omega} \frac{k_{\parallel}^2}{k^2} - \frac{\gamma - 1}{4} k_{\parallel}^2 b_{T_0}^2 \right]^2 \tilde{P}^{\rho}(k) e^{-k^2/k_F^2} \frac{k dk}{2\pi} \quad (11)$$

where  $f_{\Omega} = d \ln D / d \ln a$  with  $D$  being the linear growth factor and  $a$  the Hubble scale factor (see Peebles 1980). The three-dimensional isotropic real-space mass power spectrum is denoted by  $\tilde{P}^{\rho}(k)$ , and  $k_F$  is the scale of smoothing due to baryon-pressure i.e.  $\tilde{P}^{\rho}(k) \exp[-k^2/k_F^2]$  gives the power spectrum of the baryons. As argued by Gnedin & Hui (1998)<sup>3</sup>,  $k_F^{-1}$  should be given by  $\sqrt{2}\bar{H}(1 + \bar{z})^{-1} f_J^{-1} x_J$ , where  $x_J$  is commonly known as the

---

<sup>3</sup>The  $k_F$  here is equal to the  $k_F$  in Gnedin & Hui divided by  $\sqrt{2}$ .

Jeans scale. The latter is equal to  $\gamma k_B T_0 / 4\pi a^2 G \bar{\rho} \mu$ , where  $\mu$  is the mean mass per particle and  $\bar{\rho}$  is the mean mass density. The numerical factor  $f_J$  relating  $k_F^{-1}$  and  $x_J$  should be  $O(1)$ , its precise value depending somewhat on the reionization history (Gnedin & Hui 1998), but it should have an insignificant effect on our work here, because we are interested primarily in the large scale fluctuations.

The other smoothing scale  $k_{\parallel}^s$  should be equal to  $\sqrt{2}/b_{T_0}$  due to thermal broadening, but we can allow it to be more general to include the effect of finite resolution as well:

$$k_{\parallel}^s = \frac{\sqrt{2}}{b_{\text{eff}}}, \quad b_{\text{eff}}^2 = b_{T_0}^2 + \frac{\text{FWHM}^2}{4 \ln 2} \quad (12)$$

where FWHM is the resolution full-width-half-maximum.

The proportionality constant  $A$  for eq. (11) should be equal to  $\bar{\tau}^2$  within the context of linear theory. However, in the spirit of Croft et al. (1998), we assume the linear prediction gives the right shape but not necessarily the right amplitude for the power spectrum on large scales (see §5 for discussions). Hence,  $A$  will be left as a free constant.

Note that the integrand in eq. (11) is precisely of the form shown in eq. (2). In fact, on large scales (small  $k_{\parallel}$  as well as  $k$  i.e. small compared to  $k_{\parallel}^s$ ,  $1/b_{T_0}$  and  $k_F$ ), modulo multiplicative factors, it reduces to the famous Kaiser (1987) result, if one identifies  $[2 - 0.7(\gamma - 1)]$  with the usual galaxy-bias-factor. Interestingly, the smoothing factor  $\exp[-k_{\parallel}^2/k_{\parallel}^{s2}]$  is exactly of the form commonly used to model nonlinear redshift distortions on small scales (e.g. Peacock & Dodds 1994; Heavens & Taylor 1995, but see also Fisher et al. 1994; Cole et al. 1994). We will take advantage of this fact, and estimate the effect of small scale distortions on the inversion procedure at large scales by allowing  $k_{\parallel}^s$  to vary.

## 4.2. Inversion on Large Scales

Motivated by eq. (11), we consider the following inversion problem: how to estimate  $\tilde{P}^{\rho}$ , on large scales, from  $P^f$ , for

$$P^f(k_{\parallel}) = \int_{k_{\parallel}}^{\infty} W^{f\rho}(k_{\parallel}/k, k) \tilde{P}^{\rho}(k) \frac{k dk}{2\pi} \quad (13)$$

where

$$W^{f\rho}(k_{\parallel}/k, k) = \frac{A' \exp[-k_{\parallel}^2/k_{\parallel}^{s2}] \exp[-k^2/k_F^2]}{\left[ 1 + \frac{f_{\Omega}}{2 - 0.7(\gamma - 1)} \frac{k_{\parallel}^2}{k^2} - \frac{\gamma - 1}{4[2 - 0.7(\gamma - 1)]} k_{\parallel}^2 b_{T_0}^2 \right]^2} \quad (14)$$

where  $A'$  is a constant.<sup>4</sup>

The above  $W^{f\rho}$  is the actual distortion kernel we will use to compute  $P^f$  for some given input  $\tilde{P}^\rho$ . However, for the inversion problem ( $P^f \rightarrow \tilde{P}^\rho$ ), we will not assume we know all the parameters in  $W^{f\rho}$ , or even the precise form of  $W^{f\rho}$ , except that, on large scales, it is equal to

$$W_\ell^{f\rho}(k_\parallel/k, k) = A' \left[ 1 + \beta_f \frac{k_\parallel^2}{k^2} \right]^2, \quad \beta_f = \frac{f_\Omega}{2 - 0.7(\gamma - 1)} \quad (15)$$

The  $\beta_f$  here is the analog of the usual  $\beta$  discussed in the context of galaxy-redshift-distortions, and  $2 - 0.7(\gamma - 1)$  is the equivalent here of the galaxy-bias factor. Note that the scales of our interest are much larger than the thermal broadening width, hence the dropping of the term involving  $b_{T_0}^2$ .

In other words, for the inversion problem, we assume we know the distortion kernel in the linear regime (eq. [15], with the single parameter  $\beta_f$ ), but otherwise do not have any other information regarding the full distortion kernel  $W^{f\rho}$  (eq. [14]) on small scales. This is intended to mimic the real-life situation we find ourselves in: that we understand linear distortions rather well, but do not have a good grasp of nonlinear distortions on small scales. We will use the extra parameters in the full kernel (which we “pretend” we do not know in the inversion procedure) to simulate the effect of nonlinear distortions on our inversion procedure (in particular, the parameter  $k_\parallel^s$ , which coincides with a factor commonly used to model nonlinear distortions in galaxy surveys; see e.g. Peacock & Dodds 1994).

Let us split the integral in eq. (13) into two parts, a part that we think we understand based on perturbation theory, and a part that takes care of the small scale distortions which we do not necessarily have a good handle on:

$$P^f(k_\parallel) = \int_{k_\parallel}^{k_\star} W_\ell^{f\rho}(k_\parallel/k, k) \tilde{P}^\rho(k) \frac{k dk}{2\pi} + \int_{k_\star}^{\infty} W^{f\rho}(0, k) \tilde{P}^\rho(k) \frac{k dk}{2\pi} \quad (16)$$

where we have assumed: 1.  $W^{f\rho} \sim W_\ell^{f\rho}$  for  $k < k_\star$ ; 2.  $k_\parallel$  is sufficiently small so that  $k_\parallel/k_\star \sim 0$ . The second term on the right then plays the role of  $\Delta$  in eq. (8). As explained in the last section, the above set-up is then suitable for an inversion analysis. One can imagine obtaining  $\tilde{P}^\rho$  given  $P^f$  for some range of  $k_\parallel$ 's, by inverting the matrix  $W_\ell^{f\rho} k dk / 2\pi$  (which is restricted to its upper, or lower depending on one's convention, triangular entries by the limits of integration), treating  $\Delta$  as a free parameter or ignoring it altogether.

---

<sup>4</sup>Note that an alternative would be to group the baryon-smoothing factor  $\exp[-k^2/k_F^2]$  together with  $\tilde{P}^\rho(k)$  instead of with the rest of the terms in the distortion kernel  $W^{f\rho}$ . Our inversion procedure can then be viewed as an attempt to recover the baryon power spectrum  $\tilde{P}^\rho(k) \exp[-k^2/k_F^2]$  rather than the mass power spectrum itself  $\tilde{P}^\rho(k)$ . However, the two coincide on large scales.



Instead of doing so, we will rewrite eq. (16) into a form that is closer to the original analysis by Croft et al. (1998), thereby making manifest the differences from our procedure suggested here.

By taking the derivative of eq. (16) with respect to  $k_{\parallel}$ , it can be shown that

$$A' \tilde{P}^{\rho}(k = k_i) = -\frac{2\pi}{(1 + \beta_f)^2 k_i} \left[ \frac{dP^f}{dk_{\parallel}} \Big|_{k_{\parallel}=k_i} - 4\beta_f k_i \left( \int_{k_i}^{k_{**}} A' \tilde{P}^{\rho}(k) k^{-1} \frac{dk}{2\pi} + C_1 \right) \right. \\ \left. - 4\beta_f^2 k_i^3 \left( \int_{k_i}^{k_{**}} A' \tilde{P}^{\rho}(k) k^{-3} \frac{dk}{2\pi} + C_2 \right) \right] \quad (17)$$

where we have used the form of  $W_{\ell}^{f\rho}$  in eq. (15). The value of  $k_i$  for which we will perform the inversion would range from some maximum  $k_{**}$  to whatever small  $k_i$  (large scale) one might wish. The constraint is that  $k_{**}$  has to be sufficiently smaller than  $k_{*}$  such that condition number 2 as set out for eq. (16) is satisfied.

The constants  $C_1$  and  $C_2$  should be

$$C_1 = \int_{k_{**}}^{k_{*}} A' \tilde{P}^{\rho}(k) k^{-1} \frac{dk}{2\pi}, \quad C_2 = \int_{k_{**}}^{k_{*}} A' \tilde{P}^{\rho}(k) k^{-3} \frac{dk}{2\pi} \quad (18)$$

Assuming some values for  $C_1$ ,  $C_2$  and the starting wavenumber  $k_{**}$ , eq. (17) can be used to obtain  $A' \tilde{P}^{\rho}(k = k_i)$  for successively smaller  $k_i$ 's (at, say, evenly spaced intervals). The method adopted by Croft et al. (1998) is equivalent to keeping only the first term within the square brackets on the right hand side of eq. (17) i.e. a simple differentiation.

Because we are interested only in small  $k_i$ 's, and because  $\tilde{P}^{\rho}(k)$  generally falls rapidly with increasing  $k$ , especially at high  $k$ 's, we can choose  $k_{**}$  to be some sufficiently large value and simply set  $C_1 = C_2 = 0$ . We will see that our method is robust enough to consistently yield good agreement with the input power spectrum on large scales (small  $k_i$ ), even though one is making an error on small scales by approximating  $C_1$  and  $C_2$  as zero. Also, strictly speaking,  $k_{**}$  should be chosen to be smaller than  $k_{*}$ , which is the  $k$ -value above which the distortion kernel is no longer described by the linear kernel in eq. [15] (see also conditions for eq. [16]). We will not be careful about it, and will see that one still obtains the correct  $\tilde{P}^{\rho}$  on large scales, again because  $\tilde{P}^{\rho}$  falls rapidly with  $k$ .

For clarity let us call the method of simple differentiation following Croft et al. (1998) **method I**, and the alternative that we propose here **method II**.

Fig. 1 shows a comparison of the inversion using method I versus II. Since it is generally difficult to judge differences between power spectral shapes in a log-log plot of the power spectrum, we instead show the fractional error in the inverted power spectrum as a function

of  $k$ . The input mass power spectrum is that of a  $\Lambda$ CDM (Standard Cold-Dark-Matter) universe, with  $\Omega_m = 1$  and  $h = 0.5$ . We have chosen the parameters  $\gamma = 1.5$ ,  $k_{\parallel}^s = 0.11(\text{km/s})^{-1}$  and  $k_F = 0.12(\text{km/s})^{-1}$  in the input  $W^{f\rho}$  (eq. [14]). The latter two values correspond to the choice  $T_0 = 10^4\text{K}$  (eq. [11] & [12]). (We will later alter  $k_{\parallel}^s$  to mimic the effect of nonlinear redshift distortions.) The length scales shown correspond to those considered by Croft et al. (1998). Since we are only interested in shapes here, the power spectra are normalized to agree at  $k = 0.005(\text{km/s})^{-1}$ . It can be seen that method I gives an inverted mass power spectrum which, on large scales, is systematically less steep, or less steeply falling, than the input (i.e. the slope of the inverted power spectrum is less negative than the actual one; see Fig. 3 for a log-log plot of the power spectra).

To understand this result, let us go back to eq. (17) and rewrite it as follows, approximating  $C_1$  and  $C_2$  as zero and  $k_{\star\star}$  as effectively infinite:

$$-\frac{2\pi}{(1 + \beta_f)^2 k_i} \left. \frac{dP^f}{dk_{\parallel}} \right|_{k_{\parallel}=k_i} = A' \tilde{P}^{\rho}(k_i) + E(k_i) \quad (19)$$

$$E(k_i) \equiv -\frac{4\beta_f}{(1 + \beta_f)^2} \int_{k_i}^{\infty} A' \tilde{P}^{\rho}(k) k^{-1} dk - \frac{4\beta_f^2 k_i^2}{(1 + \beta_f)^2} \int_{k_i}^{\infty} A' \tilde{P}^{\rho}(k) k^{-3} dk \quad (20)$$

On the left hand side of eq. (19) is essentially the estimator of Croft et al. (1998; method I) for the shape of the mass power spectrum. The first term on the right is the true mass power spectrum, and  $E$  is the error of method I. Approximating a realistic power spectrum  $\tilde{P}^{\rho}(k)$  as  $k^{-n}[1 - \epsilon(k)]$  where  $\epsilon(k)$  is positive and is an increasing function of  $k$ , it is not hard to show that  $d(E/\tilde{P}^{\rho})/dk_i \geq 0$  by expanding to first order in  $\epsilon$ , which means  $E$  is decreasing with  $k_i$  slower than, or at most as fast as,  $\tilde{P}^{\rho}$  is. Eq. (19) then tells us method I would systematically give a flatter estimate of the mass power spectrum than the true one. The limiting case of  $d(E/\tilde{P}^{\rho})/dk_i = 0$  occurs when the input power spectrum  $\tilde{P}^{\rho}$  obeys a strict power-law, in which case  $E$  has the same shape as the input, and method I recovers the shape of the true power spectrum.

It can also be seen that both method I and II fail on small scales (large  $k$ ). This should come as no surprise because no attempts have been made to model the small scale effects in the inversion procedure laid out in eq. (17) (see also eq. [16]). We “pretend” that we do not know the actual full distortion kernel (eq. [14]), but instead assume only knowledge of the large scale distortion kernel (eq. [15]) when carrying out the inversion. Moreover, for method II, we have not been very careful in selecting the value of the constants  $C_1$  and  $C_2$ : we simply set them to zero.

To estimate the effect of nonlinear distortions on our inversion procedure, we decrease  $k_{\parallel}^s$  to  $0.028(\text{km/s})^{-1}$ , and show the outputs of method I and II in Fig. 2. Here we are taking

advantage of the fact that the factor of  $\exp[-(k_{\parallel}/k_{\parallel}^s)^2]$  in eq. (14) is commonly used to model nonlinear distortions in the case of galaxy surveys (see e.g. Peacock & Dodds 1994). By raising the scale of nonlinear distortion by a factor of about 4, we hope to gain an idea of how the as yet poorly understood nonlinear distortions on small scales might affect the inversion of the power spectrum on large scales. However, it remains to be checked using simulations how realistic this choice of scale, or this particular parametrization of nonlinear distortions, is. The agreement on large scales for method II is not as good as before, but is still within about 7%, and is better than that of method I. It is possible to improve the agreement by playing with the input parameters  $C_1$ ,  $C_2$  or  $k_{\star\star}$ . We will not pursue that here.

We also show in Fig. 3 what the inverted and input power spectra look like in a log-log plot. The subtle differences in the shapes of the power spectra are still possible, but harder, to discern in such a plot.

Lastly, we have assumed in all tests above that the input  $\beta_f$  (eq. [15]) is known when performing the inversion. In practice, there is an uncertainty due to the lack of knowledge of the precise values of  $\gamma$  and  $f_{\Omega}$ . In Fig. 4, we show a case where the inversion  $\gamma$  is chosen to be slightly different from the known input  $\gamma$ . (The actual value for  $\gamma$  in the real universe is likely to have a narrow range  $1.3 \lesssim \gamma \lesssim 1.6$  c.f. Hui & Gnedin 1997). The impact on the recovery of the power spectrum shape appears minimal, for the small change in  $\gamma$ . Similarly,  $f_{\Omega}$  at a redshift of around 3 should fall in a narrow range (close to 1), for reasonable values of  $\Omega_m$  and the cosmological constant today.

## 5. Conclusion

The main aim of this paper is to draw attention to the fact that redshift distortions in general make the three-dimensional redshift-space mass power spectrum anisotropic, and so the inversion from the projected one-dimensional redshift-space transmission power spectrum to the three-dimensional real-space mass power spectrum involves more than a simple differentiation (eq. [2]). Given a kernel ( $W^{f\rho}$  in eq. [6]) that relates the relevant power spectra, it is possible to perform the inversion by essentially inverting a triangular matrix proportional to  $W^{f\rho}$  (eq. [7] & [8]).

We have demonstrated this idea with a kernel  $W^{f\rho}$  that is motivated by linear perturbation theory. In general, we find that a simple differentiation method tends to make the inverted three-dimensional real-space power spectrum flatter than it really is on large scales. A procedure that remedies this is outlined in eq. (17). We have referred to the former (straightforward differentiation) as method I, and the latter as method II.

As we have remarked before in §4.2, if the three-dimensional real-space mass power spectrum  $\tilde{P}^\rho(k)$  obeys a strict power-law, the simple differentiation procedure of method I will recover the same power-law. That we observe a deviation of the method-I-inverted power spectrum from the input in Fig. 1 to 4 is a reflection of the fact that a realistic power spectrum (such as CDM) is only well-approximated by a power-law for narrow ranges of  $k$ . The differences between method I and II are not easy to discern in a log-log plot such as the one shown in Fig. 3, especially when one is dealing with observed or simulated data with noise. The systematic error of method I is nonetheless present, and more easily seen in plots such as the one in Fig. 2. A cursory inspection of some of the log-log plots of the inverted power spectrum in Croft et al. (1998) seems to indicate that method I does give a slightly flatter power spectrum compared to the input on large scales, but it certainly should be more carefully quantified with simulations.

An interesting consequence of redshift-space distortions is that the one-dimensional transmission power spectrum  $P^f$  is no longer guaranteed to be monotonically decreasing (Kaiser & Peacock 1991), unlike in the case where the distortion kernel is trivial (i.e. set  $W^{f\rho}$  to constant in eq. [13]). Method I, where  $P^f$  is simply differentiated to obtain the mass power spectrum  $\tilde{P}^\rho$ , could then give a negative mass power spectrum and fail dramatically (see eq. [19], and discussions that follow).

For a power-law mass spectrum with  $\tilde{P}^\rho(k) \propto k^{-n}$ , it is simple to show using the linear distortion kernel (eq. [15]), together with eq. (13), that  $dP^f/dk_\parallel > 0$  if  $[-\sqrt{\beta_f^2 + 6\beta_f + 1} - (1 - \beta_f)]/(1 + \beta_f) < n < [\sqrt{\beta_f^2 + 6\beta_f + 1} - (1 - \beta_f)]/(1 + \beta_f)$ . For the parameters  $\Omega_m = 1$  and  $\gamma = 1.6$ , which were adopted by Croft et al. (1998), this implies a range of  $-1.62 < n < 1.17$ , within which method I should give a negative inverted mass power spectrum. Of course, a strict power-law power spectrum with  $n$  in such a range is not very interesting because it gives a diverging one-dimensional transmission power spectrum ( $n > 2$  is required for convergence). It is for this reason that a direct comparison cannot be made between the above simple estimates and a test-case shown by Croft et al. (1998) in which the initial power spectrum has  $n = 1$ . In fact, for a scale-free initial power spectrum of  $k^{-n}$ , the stable-clustering mass power spectrum at high  $k$  should be  $k^{-6/(5-n)}$  (Peebles 1980). For  $n = 1$ , this means the high  $k$  mass power spectrum asymptotes to  $k^{-1.5}$ , which is still not enough to regularize the integral for the transmission power spectrum (eq. [13] together with eq. [15]). It is likely that in their test-case, an effective ultraviolet cut-off is imposed by the finite resolution of the simulation, or else the true nonlinear redshift-distortion kernel provides an effective regularization. Note, however, that there is no small-scale Jeans smoothing to help here because Croft et al. (1998) used N-body-only simulations.

Nonetheless, we should emphasize that while, on large scales, the direction of the sys-

tematic error of method I is on firm ground (i.e. systematic flattening), the size of the error, on the other hand, is subject to further investigation. We have used linear theory in §4 to estimate the magnitude of this effect. The linear calculation gives us the effective “bias-factor” (let us call it  $b_\beta$ , which equals  $2 - 0.7(\gamma - 1)$  in eq. [15]) associated with the distortion parameter  $\beta_f$  (i.e.  $\beta_f = f_\Omega/b_\beta$ ), but this might not be the correct  $b_\beta$  in the presence of nonlinear fluctuations on small scales.

For instance, according to arguments by Scherrer & Weinberg (1997), the galaxy-bias  $b_g$  (different from  $b_\beta$  above, see below), defined as the ratio of the galaxy to mass two-point function on large scales (where galaxy is related to mass by a local transformation), generally involves all the higher derivatives of the local transformation around  $\delta = 0$  i.e. not just the first derivative, as is in the case of a linear perturbative calculation.

One might naively think that, in the case of the Lyman-alpha forest,  $b_\beta$  should be set equal to the analog of the galaxy-bias defined above, namely the ratio of the transmission to mass power spectrum on large scales. Let us denote this latter quantity also by  $b_g$ . This number is smaller than 1 in our case (because the exponential ( $e^{-\tau}$ ) suppresses large fluctuations), which means the redshift distortions are more pronounced than we have assumed in §4, and the systematic error of method I should be even larger!

However, there are at least two reasons to suspect that this is not the correct conclusion. First, as emphasized recently by Dekel & Lahav (1998), the bias factor that shows up in the linear distortion kernel ( $b_\beta$ ) is not necessarily the same as  $b_g$  defined above, because of the nonlinearity of the biasing transformation (see below for a discussion of the transformation relevant in our case; we do not suffer from stochastic biasing, however). In fact, according to Dekel & Lahav, even the form of the linear distortion kernel could be slightly modified (see also Pen 1997).

A second, perhaps more important, reason is that the mapping from the mass density field  $\rho$  to the transmission  $f$  actually involves two local “biasing” transformations with the redshift-space distortion in between. First<sup>5</sup>, the mass density in real-space is related to the neutral hydrogen density in real-space through the local transformation  $n_{\text{HI}} \propto \rho^{2-0.7(\gamma-1)}$ ; second, this is then “distorted” into the optical depth in redshift-space through  $\tau \propto [\rho^{2-0.7(\gamma-1)}]_z$ , where  $[\ ]_z$  denotes a quantity in redshift-space; finally, another local transformation maps the optical depth in redshift-space to the transmission in redshift-space:  $f = e^{-\tau}$ . It is plausible that the first two steps determine the correct value of  $b_\beta$ , while the last merely shifts the overall normalization of the final redshift-space power spectrum of the transmission on large scales (see Hui 1998).

---

<sup>5</sup>We ignore the spatial dependence of the thermal profile to simplify the discussion here; see eq. (9).

Lastly, there is of course the possibility that even the form of the large-scale distortion kernel in eq. (15) might be incorrect, or as is more likely the case, that the linear distortion kernel applies only at (a small range of) the largest scales (see e.g. Cole et al. 1994). This is related to the question of how nonlinear clustering on small scales, or translinear clustering on intermediate scales, affects the large scale behaviour of redshift distortions. Couple this with the effects of nonlinear local transformations: we indeed have a complicated problem here. Some of these issues are beginning to be addressed (see Fisher & Nusser 1996; Taylor & Hamilton 1996; Scoccimarro 1998; Hui et al. 1998 for the former, and Scherrer & Weinberg 1997; Dekel & Lahav 1998; Hui 1998 for the latter). The good news, at least in the case of the Lyman-alpha forest, is that the form of the relevant local “biasing” transformation is known exactly.

Both issues, the problem of translinear or nonlinear redshift-space distortions and the problem of biasing in real as well as in redshift-space, are obviously of great interest in the wider context of large scale structure and galaxy surveys. Analytical calculations, with reality checks using simulations, would be necessary to address these questions. We hope to pursue aspects of these issues in a future publication.

As this paper was nearing completion, the author became aware of a preprint by Nusser & Haehnelt (1998) who also considered the effects of redshift-space distortions on the forest, not in the case of inversion from the transmission power spectrum to the mass power spectrum, but in the case of the recovery of the mass density field itself. The author thanks Rupert Croft and Albert Stebbins for useful discussions. This work was supported by the DOE and the NASA grant NAG 5-7092 at Fermilab.

## References

- Cole, S., Fisher, K. B., & Weinberg, D. H., 1994, MNRAS **267**, 785+
- Croft, R. A. C., Weinberg, D. H., Katz, N., & Hernquist, L., 1998, ApJ **495**, 44+
- Dekel, A. & Lahav, O., 1998, preprint, astro-ph 9806193
- Fisher, K. B., Davis, M., Strauss, M. A., Yahil, A., & Huchra, J. P., 1994, MNRAS **267**, 927+
- Fisher, K. B. & Nusser, A., 1996, MNRAS **279**, L1,
- Gnedin, N. Y. & Hui, L., 1998, MNRAS **296**, 44+
- Hamilton, A. J. S., 1997, astro-ph 9708102
- Heavens, A. F. & Taylor, A. N., 1995, MNRAS **275**, 483
- Hui, L., 1998, in preparation
- Hui, L. & Gnedin, N. Y., 1997, MNRAS **292**, 27

- Hui, L., Gnedin, N. Y., & Zhang, Y., 1997, *ApJ* **486**, 599+
- Hui, L., Kofman, L., & Shandarin, S., 1998, in preparation
- Hui, L. & Rutledge, R. E., 1997, preprint, astro-ph 9709100
- Kaiser, N., 1987, *MNRAS* **227**, 1
- Kaiser, N. & Peacock, J. A., 1991, *ApJ* **379**, 482
- Miralda-Escude, J. & Rees, M., 1993, *MNRAS* **260**, 617+
- Nusser, A. & Haehnelt, M., 1998, preprint, astro-ph 9806109
- Peacock, J. A. & Dodds, S. J., 1994, *MNRAS* **267**, 1020+
- Peebles, P. J. E., 1980, *The Large Scale Structure of the Universe*, Princeton University Press
- Pen, U., 1997, preprint, astro-ph 9711180
- Rybicki, G. B. & Lightman, A. P., 1979, *Radiative Processes in Astrophysics*, John Wiley & Sons
- Scherrer, R. & Weinberg, D., 1997, preprint, astro-ph 9712192
- Scoccimarro, R., 1998, in preparation
- Taylor, A. N. & Hamilton, A. J. S., 1996, *MNRAS* **282**, 767

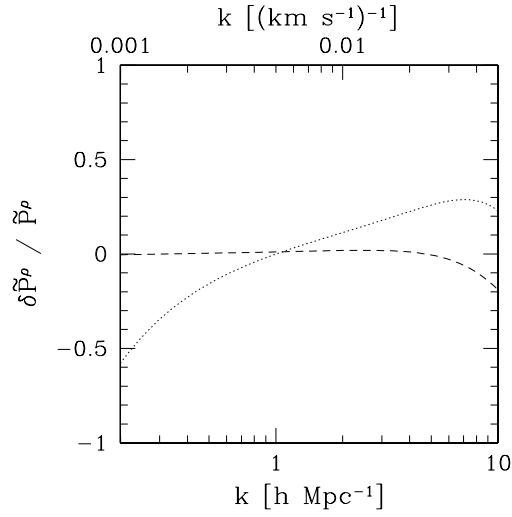


Fig. 1.— A comparison of the Croft et al. (1998) inversion (method I; *dotted line*) versus inversion set forth in eq. (17) (method II; *dashed line*). On the y-axis is  $\delta\tilde{P}^\rho/\tilde{P}^\rho$  where  $\delta\tilde{P}^\rho = \tilde{P}_{\text{output}}^\rho - \tilde{P}^\rho$ , and  $\tilde{P}^\rho$  is the input real-space mass power spectrum, and  $\tilde{P}_{\text{output}}^\rho$  is the output. The input power spectrum is that of the SCDM model, and the input parameters are  $\gamma = 1.5$ ,  $k_{\parallel}^s = 0.11(\text{km/s})^{-1}$  and  $k_F = 0.12(\text{km/s})^{-1}$  (eq. [14]). The inversion parameters are  $k_{**} = 0.14(\text{km/s})^{-1}$ ,  $C_1 = C_2 = 0$  (eq. [17]). The inversion  $\beta_f$  is assumed to be the same as that in the input (i.e.  $1/1.65$ , see eq. [15]). The outputs are normalized to match the input at  $k = 0.005(\text{km/s})^{-1}$ .



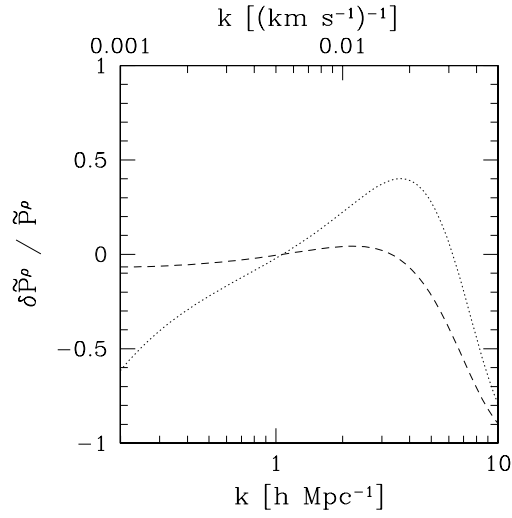


Fig. 2.— Same as Fig. 1 except that  $k_{\parallel}^s = 0.028(\text{km/s})^{-1}$ .

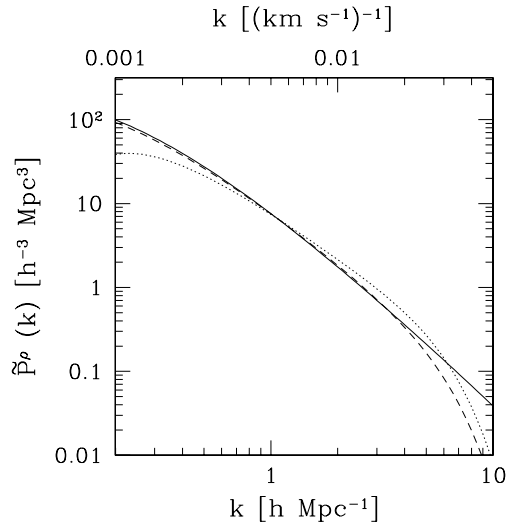


Fig. 3.— The solid line is the input linear power spectrum. The dashed line is the output by using method II (eq. [17]), and the dotted line is the output by using method I i.e. simple differentiation. The parameters are the same as in Fig. 2.

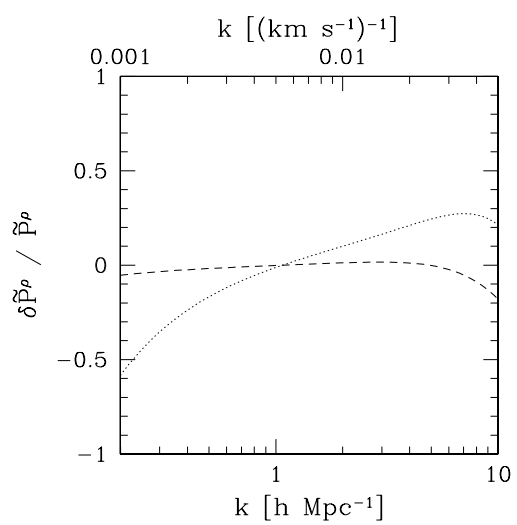


Fig. 4.— Same as Fig. 1 except that the inversion  $\gamma - 1$  is chosen to be 0.3 instead of the input value 0.5.